

A System for Generating Non-Uniform Random Variates using Graphene Field-Effect Transistors

Nathaniel J. Tye

Cambridge Graphene Centre,
Department of Engineering,
University of Cambridge
njt48@cam.ac.uk

James T. Meech

Department of Engineering
University of Cambridge
jtm45@cam.ac.uk

Bilgesu A. Bilgin

Department of Engineering
University of Cambridge
bab46@cam.ac.uk

Phillip Stanley-Marbell

Department of Engineering
University of Cambridge
phillip.stanley-marbell@eng.cam.ac.uk

Abstract—We introduce a new method for hardware non-uniform random number generation based on the transfer characteristics of graphene field-effect transistors (GFETs) which requires as few as two transistors and a resistor.

We implement the method by fabricating multiple GFETs and experimentally validating that their transfer characteristics exhibit the nonlinearity on which our method depends. We use characterisation data in simulations of a proposed architecture for generating samples from dynamically selectable non-uniform probability distributions. The method we present has the potential for Gb/s sample rates, is reconfigurable for arbitrary target distributions, and has a wide range of possible applications.

Using a combination of experimental measurements of GFETs under a range of biasing conditions and simulation of the GFET-based non-uniform random variate generator, we demonstrate a speedup of Monte Carlo integration by up to $2\times$. This speedup assumes the analog-to-digital converters reading the outputs from the circuit can produce samples in the same amount of time that it takes to perform memory accesses.

Index Terms—Monte Carlo Accelerator, Non-Uniform Random Variates, Graphene, Graphene Transistors

I. INTRODUCTION

Hardware *uniform random number generators* exist in both research and commercial computer architectures, with generation rates of up to 6.4 Gb/s [13]. Uniform random numbers are widely used in applications such as cryptography, where the objective is to generate bit vectors (e.g., 256-bit vectors) that are uniformly distributed over some range and are therefore difficult to guess. In contrast, this article focuses on *programmable random variate accelerators* (PRVAs) for generating *non-uniform random variates* (NRVs), random samples chosen from a non-uniform probability distribution.

A. Applications of Non-Uniform Random Variates

Many important applications in science and engineering depend not on uniform random samples, but instead require NRVs, from a wide range of distributions. Applications of NRVs range from Monte Carlo simulations [28], to quantitative finance [36] to particle filter localisation for driverless cars [38]. NRVs are also important in Bayesian machine learning applications [18], which involve the computation of a marginal probability which goes into the denominator of the expression of Bayes' rule. Computing these marginal probabilities in turn requires evaluating an integral of a probability distribution. Because the distributions in question are typically high-dimensional and

have no known analytic equational form, their integration often requires Monte Carlo integration methods where one samples repeatedly from the corresponding distribution.

B. Challenges

Because generating samples from distributions whose inverse cumulative distribution function (CDF) does not have a closed form requires time-consuming accept-reject sampling [6], generating random samples from non-uniform distributions is typically an order of magnitude slower and less energy-efficient than generating uniformly distributed random samples [37]. One promising direction for efficiently generating NRVs is to sample from a physical process whose evolution in time [43] or noise characteristics [26] follow some known and (ideally) controllable probability distribution.

C. Contributions

This article presents the first demonstration of generating NRVs by exploiting properties of graphene field-effect transistors (GFETs) previously considered undesirable: their ambipolar transfer characteristics and their lack of a band gap. We provide a tutorial overview of the properties of GFETs (Section II) and introduce a circuit topology for using a chain of GFETs together with a uniform random variate generator to generate dynamically controllable non-uniform distributions (Section III). We present the methodology we used for fabricating an array of GFETs and empirically characterising their transfer characteristics (Section IV) and we use those empirically measured GFET transfer characteristics to demonstrate the proposed method in a simulated combined circuit topology (Section V). We then use the generated NRVs in an end-to-end system example, where we evaluate their benefit to speeding up Monte Carlo integration, as well as their benefit to reducing the error in the Monte Carlo integration process (Section VI).

II. PROPERTIES OF GRAPHENE FIELD-EFFECT TRANSISTORS

GFETs have a channel made of single- or multi-layer graphene, rather than a semiconducting material such as silicon or germanium [33]. Unlike traditional semiconductors, graphene is a semi-metal: it lacks a band gap and its conduction

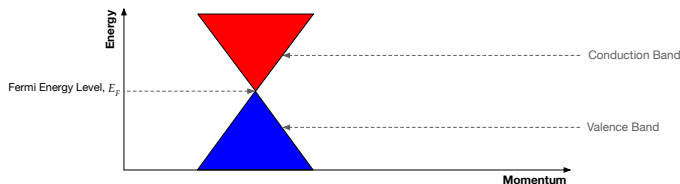


Fig. 1. Energy band structure of graphene, showing the Dirac point, where the conduction and valence bands touch. E_F is the Fermi level. In undoped/unbiased graphene, it is located at the Dirac point. There is no band gap: GFETs have low on- to off-current ratios making them a poor choice for traditional digital logic applications [16].

and valence bands don't overlap. Instead, the conduction and valence bands meet at the *Dirac point* (Figure 1).

Electrons at the Dirac point are effectively massless and so have unusually high electron mobilities. As a result, the phonon-limited carrier mobility (the highest possible mobility limited by interactions between carriers and vibrations of the channel's crystal lattice) of graphene on SiO_2 is predicted to be as high as $200,000 \text{ cm}^2 \text{ V}^{-1} \text{ s}^{-1}$ [4]. Although high electron mobilities result in more efficient flow of charge, the lack of a band gap means GFETs have low on- to off-current ratios and can never completely turn off, making them unsuitable for digital logic applications [16].

The poor on- to off-current ratios of GFETs in digital logic applications does not preclude their use in other areas of computing. Because it is possible to tune the Fermi level in graphene (which typically lies at the Dirac point) by biasing the channel, it is possible to control device characteristics, e.g., using multi-gate structures, in a manner not equally possible in typical metal-oxide-semiconductor field-effect transistors (MOSFETs). GFETs also have transfer characteristics that are non-linear and different to MOSFETs: as the gate voltage is swept, the drain current exhibits a v-shaped characteristic curve, with the conductance decreasing until it reaches a minimum value before increasing again.

III. A GFET NON-UNIFORM RANDOM VARIATE GENERATOR

If the signal at the gate of a GFET is a uniform random voltage distribution, then the distribution of the drain current will be modified by the GFET's transfer characteristics. The exact shape of the transfer characteristics varies with the source-drain voltage V_{DS} . Thus, for a uniform random voltage distribution at the gate, varying V_{DS} for a GFET changes the distribution of drain currents. If these drain currents are converted to a voltage and applied to additional GFETs, it is possible to combine the transfer characteristics and biasing of multiple GFETs to achieve a range of drain current (and hence voltage) distributions.

Figure 2 shows a possible circuit to implement generation of a controllable non-uniform voltage distribution using GFET properties. Each GFET in Figure 2 has a bias voltage, V_{DS} , that controls its transfer characteristics. The first GFET has a uniformly distributed random voltage across its gate and a corresponding distribution of drain currents, with the values of the drain currents for each input voltage determined by the transfer characteristics of the GFET at its bias voltage $V_{DS}^{\text{GFET}_1}$. The circuit in Figure 2 converts the drain current of the first

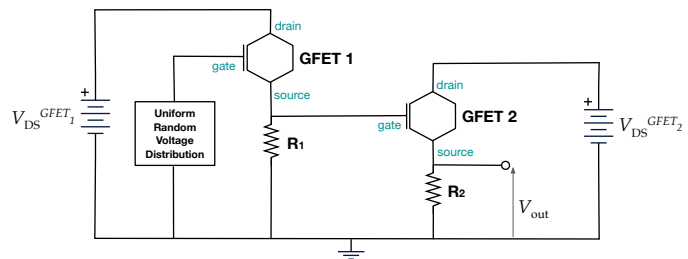


Fig. 2. Example schematic of a possible circuit used to transform a random uniform noise distribution (V_1) into an arbitrary distribution by cascading several individually biased GFETs.

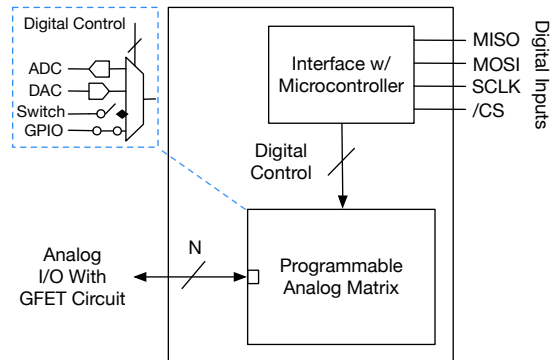


Fig. 3. Schematic of integration hardware used with the GFET circuits, based on the schematic of the Maxim MAX11300 [25]. The N signal analog I/O connects to each terminal of each GFET. The zoomed view shows circuitry within the programmable analog matrix for control of each terminal. The switch determines whether the channel is enabled, the ADC converts an analog signal into a digital signal read by the CPU, the DAC converts a digital signal from the CPU to an analog signal for the GFETs. The GPIO ports function as inputs/outputs with a controllable logic level, e.g. for setting a bias level. All of these are run into a MUX which is digitally controlled by the microcontroller.

GFET into a voltage input to the gate of the second GFET, using a resistor, R_1 . In practice, using a transimpedance amplifier (TIA) to perform this current-to-voltage conversion would result in less Johnson-Nyquist noise in the generated voltages, though the presence of such noise may not be detrimental given our goal of generating random variates. The analyses that follow in Section V therefore use a resistor for converting the drain currents to voltages to control the second stage in the circuit. The second GFET in Figure 2, operating at a bias voltage of $V_{DS}^{\text{GFET}_2}$, further shapes the distribution of the output signal. By selectively connecting multiple GFETs in the manner of Figure 2 (and possibly using multi-gate GFETs), this method in principle permits generation of a final output V_{Out} with a range of selectable distributions, controlled by the combination of R_1 , $V_{DS}^{\text{GFET}_1}$, and $V_{DS}^{\text{GFET}_2}$.

A. Integration with an Existing Computer Architecture

For integration into a larger system, we propose the use of a programmable analog switching matrix, e.g., a MAX11300 [25], such as that illustrated in (Figure 3). This serves as an interface between an external processor and the GFET die and allows for dynamic reconfiguration of the GFET circuit. We present a hardware prototype of this analog switching matrix in Section IV.

The GFET random number generator could be integrated into a package with an existing CPU and ADC using bond wires to connect the two separate dies. Figure 4 shows a block diagram

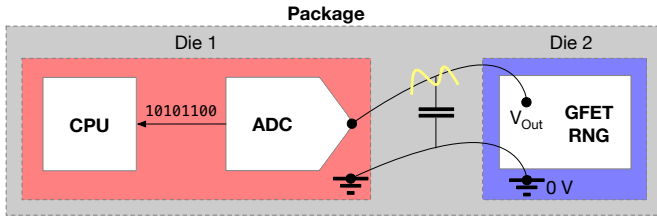


Fig. 4. Connection of CPU and random number generator die using bond wires with resistance R across them and capacitance C between them.

of the arrangement. The maximum frequency at which the bond wire can change state depends on the RC time constant.

B. Wavelet Decomposition and Reconstruction of Distributions

In signal processing, the Fourier transform decomposes a time-varying signal into its constituent frequency components and the Fourier series allows for the construction of an arbitrary signal from a sum of sines and cosines. This is a special case of wavelet analysis, which allows for any function to be described by a set of orthonormal basis functions.

Wavelet analysis uses an analysing wavelet with a scaling function to generate a set of basis functions. These basis functions are simply scaled and shifted versions of the analysing wavelet [9]. The inner product of the scaling and wavelet functions, which are necessarily orthogonal, gives a matrix of wavelet coefficients.

The discrete wavelet transform (DWT) uses known scaling and wavelet functions to generate a known set of basis functions. When applied to a discrete signal, those basis functions give an approximation of the signal, characterised by its wavelet coefficients [5]. The inverse transform is simply the linear combination of these basis functions, and thus allows for reconstruction of the original signal with a desired level of accuracy dependent on the number of coefficients used.

We demonstrate wavelet decomposition and reconstruction of a distribution in the following example. We show the distributions reconstructed from inverse DWTs with different numbers of coefficients, corresponding to a given level of accuracy for the lognormal distribution in Figure 5. We used a second-order Coiflet wavelet for both the DWT and the inverse-DWT. We chose this wavelet arbitrarily as a proof-of-concept for the proposed method, but it appeared to give reasonable results. We calculated the Kullback-Leibler (KL) divergence [17], a measure of the closeness of two distributions. Figure 5(b) uses the most coefficients and was thus the most accurate reconstruction, with a calculated KL divergence of 0, an identical reconstruction. Figure 5(c) used less than half the coefficients of (b) and had a KL divergence of 1.19. Figure 5(d), which used less than a quarter of the coefficients of (b) was actually closer than (c), with a KL divergence of 0.45. Figure 6 is a block diagram of a proposed complete system. Section IV and Figure 7 (c) present an early prototype of this system.

We have shown that a distribution can be reconstructed from a set of wavelet coefficients determined by a wavelet transform. If we consider these coefficients to be bias voltages for GFETs, which have a tunable characteristic transfer function with a certain distribution, then the characteristic of a GFET can be

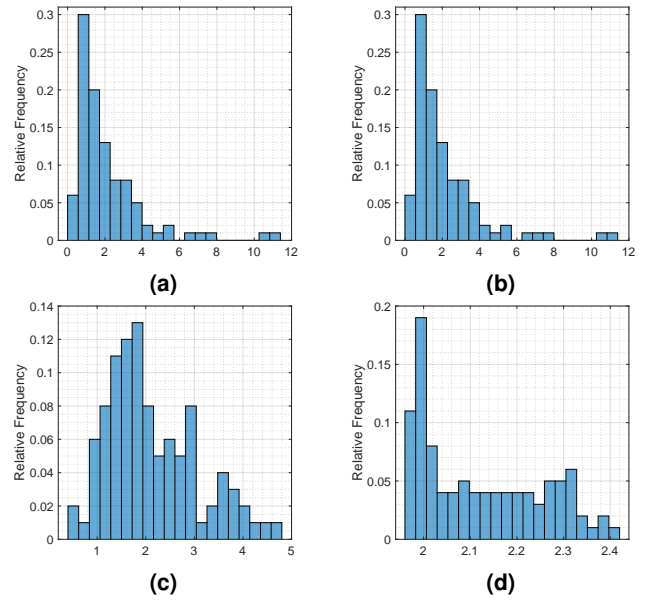


Fig. 5. (a) A software-generated lognormal distribution; (b) reconstructed distribution using 55 coefficients; (c) reconstruction using 22 coefficients; (d) reconstruction using 12 coefficients. In each case, the x-axis is simply a number.

considered as an analysing wavelet, with the bias voltages being the scaling parameters. Summing the output of each GFET (or combination of GFETs), with each representing a basis function, in principle, allows for the reconstruction of any arbitrary function, with the accuracy dependent on the number of GFETs used.

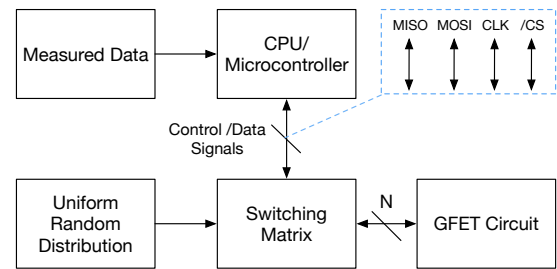


Fig. 6. Proposed system to sample from non-uniform distributions. A CPU processes some data and takes the DWT, then converts the DWTs scaling parameters into control signals, e.g., bias voltages and configurations of GFETs. The architecture inputs a uniform random variate to the GFET circuit, which transforms it into an approximation of the target distribution. The CPU then reads the approximated distribution from the circuit output.

IV. GFET FABRICATION AND ELECTRICAL CHARACTERISATION

GFETs in the results presented here consist of an Si substrate onto which we patterned a gold back gate. We grow a 60 nm alumina (Al_2O_3) layer by atomic layer deposition (ALD), onto which we transfer a monolayer of graphene using a wet transfer process. This graphene monolayer was grown by chemical vapour deposition (CVD) and purchased from Graphenea Inc [8]. After patterning the graphene, we deposit the gold source and drain contacts onto the graphene to create a $40 \mu\text{m} \times 40 \mu\text{m}$ GFET channel that lies exactly above the back gate. The large feature size compared to GFETs in the literature (channel lengths below 100 nm [21]) is for ease of

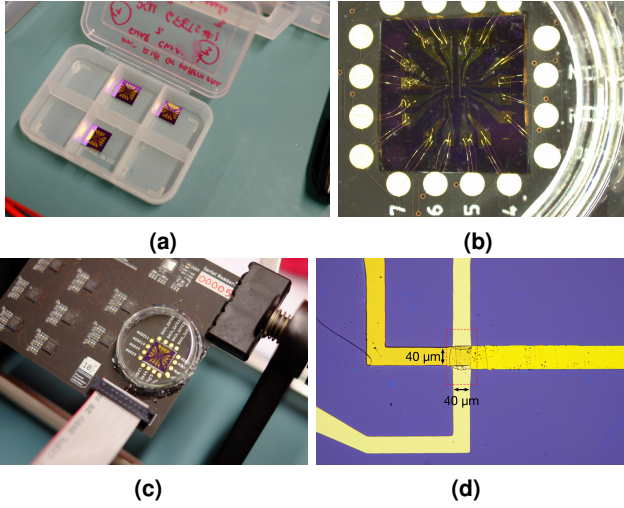


Fig. 7. (a) Three GFET array dice, each comprising four GFETs each having source, drain, top gate and back-gate contacts; (b) complete GFET die used in this investigation; (c) the custom PCB for dynamic reconfiguration of GFET circuits; (d) microscope image of the GFET investigated in this paper.

fabrication and testing. The electrical performance is beyond the scope of this work; tunability and properties of GFETs are the focus here. The channel is insulated by another layer of alumina, onto which we pattern gold top gates aligned with the GFET channels. We electrically passivate the whole device using a final ALD deposition of alumina. Finally, to facilitate electrical access to the GFETs, we etch away the alumina on top of the contacts that are electrically linked to the source, drain, back, and top gates of the GFETs.

We fabricate four identical GFETs on each silicon die (Figure 7(a)) and we electrically connect the GFETs via wire-bonding the die from its gold contacts (Figure 7(b)) to a custom printed circuit board (PCB) (Figure 7(c)). The PCB comprises an array of DACs, ADCs, and analog switches, all of which allow for dynamic and in-situ (re)configuration of a given circuit. Because graphene is sensitive to atmospheric effects¹, and also to protect the wire-bonding, we place a glass protective cover over each die once bonded to the PCB, sealed with hot glue. The hardware prototype in Figure 7(c) implements the GFETs required to realise the circuit in Figure 2, as well as the analog switching matrix described in Figure 3.

We performed electrical characterisation of the GFETs using two Keithley 2450 source-measure units (SMUs) synchronised using TSP-link. Figure 8(a) shows the transfer characteristic characterisation results of fabricated GFETs, with data obtained by conducting a linear sweep of the (top) gate-source (V_{GS}) voltage between -10.0 V and $+10.0$ V in both forward and reverse directions and measuring the resultant drain current (I_{DS}). Each curve shows the transfer characteristic for a constant source-drain bias voltage (V_{DS}), which we updated for each measurement.

¹In principle, atmospheric effects can lead to doping of the channel. These effects should however not occur even in the absence of the sealed glass protective cover, as we fabricated the devices in a cleanroom environment and encased the graphene in alumina as described above. We however cannot rule out inadvertent doping as a result of the fabrication process.

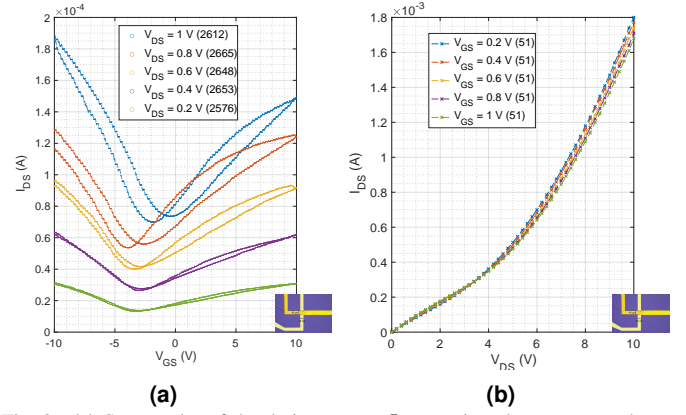


Fig. 8. (a) Scatter plot of the drain current, I_{DS} against the top gate voltage, V_{GS} , for different bias voltages of V_{DS} ; (b) plot of the drain current, I_{DS} against the source-drain voltage, V_{DS} for a stepped gate-source voltage V_{GS} . The number of datapoints for each measurement is in brackets in the legend.

The Dirac points in Figure 8(a) lie to the left of 0.0 V, which suggests an n-type doping of the graphene channel. The deepening of the valley with increasing bias voltage V_{DS} is a commonly-observed characteristic in GFETs [15], as is the hysteresis in the transfer characteristics, which the measurements of Figure 8 (a) show for all applied bias voltages. This hysteresis is a result of multiple phenomena: charge trapping between the graphene channel and the insulating layers are a major cause [20], however, additional factors include capacitive gating causing a negative shift and charge transfer causing a positive shift [41] in the conductance with respect to gate voltage.

We also measured the I_{DS} versus V_{DS} characteristics of the GFETs while varying the gate voltage V_{GS} between 0.2 V and 1.0 V, for source-drain voltages V_{DS} over the range 0.0 V to 10.0 V. Traditional MOSFETs exhibit saturation of their I_{DS} versus V_{DS} characteristics, with the characteristics separated into two main operating regions: linear and nonlinear. In GFETs however, this saturation does not appear, due to a combination of graphene's lack of a band gap and Klein tunnelling [27]. Figure 8(b) shows the measured characteristics for the GFET.

The characterisation data in Figure 8(b) indicate that the devices switch from a relatively linear region of conductance to a nonlinear region at a bias voltage of around 3.5 V. This is in line with previous results which show that GFETs, in comparison to MOSFETs, often have a second linear region; there is a point of inflection [33] which appears to be the case in the plots here, at a V_{DS} of approximately 3.5 V.

As we show in Section V, the nonlinearity of the GFET transfer characteristics, combined with the tunability of the characteristic shape by controlling V_{DS} allows us to use one or more GFETs to transform uniform distributions of V_{GS} into non-uniform distributions of I_{DS} .

V. SIMULATIONS OF GFET CIRCUITS

We use the GFET characterisation data from Section IV to simulate possible topologies for the GFET-based PRVA of Figure 2, using a custom-built simulation model of the circuit, implemented in Mathematica. We use an interpolating function whose values are determined from the measured GFET transfer

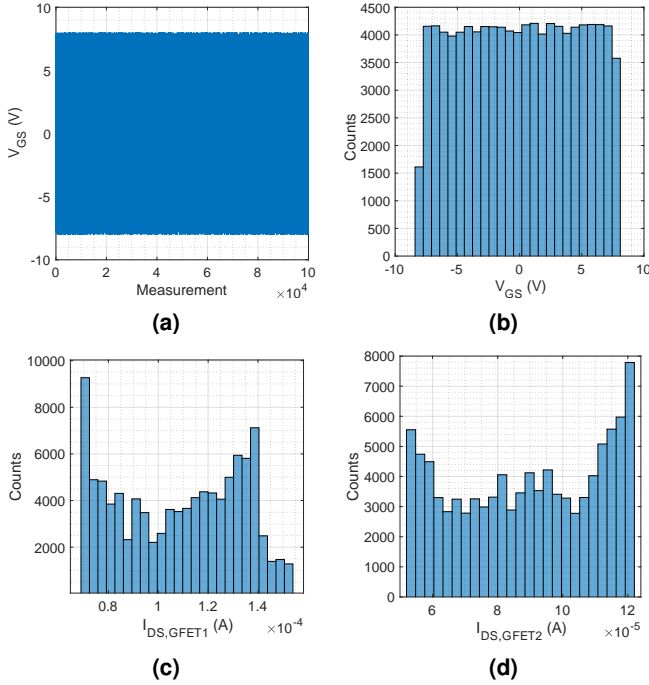


Fig. 9. (a) Example of a generated uniform pseudo-random voltage distribution used the simulation; (b) histogram of the voltage distribution. (c) and (d) show histograms of the GFET current distributions for biases of 1 V and 0.8 V respectively.

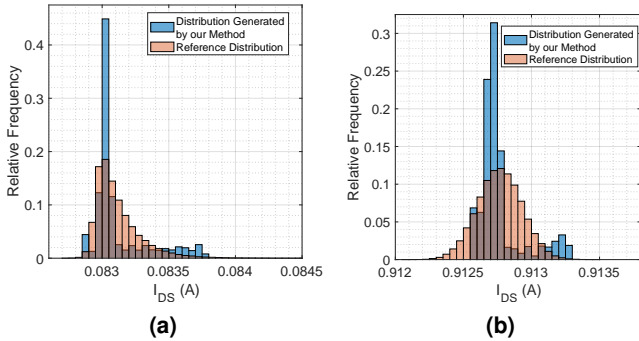


Fig. 10. Histograms of simulated transformations of uniform to non-uniform distributions. (a) GFET-only based transformation with a reference Burr Type-XII; (b) Combined GFET and computational transform with reference lognormal.

characteristics and stimulate the gate of the first GFET in the circuit with a uniform random distribution between -8 and $+8$, effectively a V_{GS} voltage in the range -8 V to $+8$ V. Figure 9 shows the time series of the uniform random voltages and their corresponding histogram distribution. We pass the output of the model of the first GFET, which is its drain current, through a modelled resistor which converts the drain current into a voltage. We then apply this voltage to the model of the second GFET of Figure 2, which we again model by encapsulating our experimental measurement data in another interpolating function. We apply the drain current of the second GFET through another resistor to obtain the output voltage.

We used the characteristics of the GFET in Figure 8 for simulations here. For the first GFET, we used the characteristic for a 0.8 V bias and for the second GFET, we used the characteristic for a 1 V bias. We use a resistance of 2.2 k Ω for

the first resistor and of 1 k Ω for the output resistance. Figure 9 (c) shows the distribution of currents from the first GFET, and Figure 9 (d) shows the distribution for the second GFET. Figure 10 (a) shows final output distribution (i.e., the output of the first GFET passed through the second GFET).

We investigated the possibility of combining the GFET-based distribution with additional subsequent software transformation by running a second simulation of the circuit in Figure 2 using the experimentally measured GFET data, with the characteristic for a 1 V biased GFET as the first GFET and the characteristic for a 0.8 V biased GFET as the second GFET. We chose a resistance of 1.2 k Ω for the first resistor and 1 k Ω for the output resistance. The initial output distribution was skewed to the right, and so we took the complementary cumulative distribution function, $\bar{F}(x)$, given by:

$$\bar{F}(x) = 1 - F(x), \quad (1)$$

where $F(x)$ is the output distribution of the circuit. To compare the similarity of the generated distribution to a genuine lognormal, we calculated the mean (μ) and standard deviation (σ) of the logarithm of the simulation output and used these as parameters to generate a lognormal distribution over the same input space. Figure 10 (b) shows histograms of the simulation output and the reference distribution.

VI. END-TO-END EXAMPLE: MONTE CARLO INTEGRATION

It is common to integrate un-normalised non-uniform density functions to convert them to valid probability density functions [36]. Monte Carlo integration is a convenient way of doing this. Consider a thought experiment where we have collected a one-dimensional dataset. The data describes the probability that indoor air quality is below acceptable levels given the reading from a volatile organic compound gas sensor. This dataset is well described by a lognormal distribution. We calculate the mean μ and standard deviation σ of the data. Before we can interrogate the data to ask questions such as ‘‘What is the probability that the air quality is unacceptable given that the sensor reading is 25?’’, we must find a normalisation constant to ensure that the probability density function integrates to one. The normalisation requires the integration of a lognormal distribution $f(x)$ where Z is an unknown normalising constant, $\mu = 0$ is the mean and $\sigma = 0.25$ is the standard deviation:

$$f(x) = \frac{Z}{x} e^{-\frac{(\ln(x)-\mu)^2}{2\sigma^2}}. \quad (2)$$

Let E be the error of the Monte Carlo integration and t be the time taken by the integration. Let N be the number of random samples used in the integration and D be the distribution that we sample from. Let A be the area of each rectangle used in the integration and b and h be the corresponding rectangle base and height. Algorithm 1 shows the integration scheme.

We repeated the integration with D as: 1) a hardware-generated lognormal distribution and 2) a lognormal distribution generated with the C++ standard library utility for generating lognormal variates, with the same μ and σ as f . We also

performed the integration with D as a uniform distribution generated with the C++ standard library random number generator, with various ranges. We assume that samples from the hardware lognormal generator can be generated in the time required for one memory access. We ran all simulations on a 2.8 GHz Intel Core i7 CPU using OpenMP parallelisation to utilise all eight processor threads.

Algorithm 1: Monte Carlo integration. Array index begins at zero.

Result: Error E and time t

Timer start

Generate N random samples from distribution D

Sort N random samples

for $i = 1$ **to** N **do**

$b = \text{Samples}[i] - \text{Samples}[i - 1]$

$h = (\text{f}(\text{Samples}[i]) + \text{f}(\text{Samples}[i - 1]))/2$

$A+ = b * h$

end

$E = |1 - A|$

Timer stop

$t = \text{stop} - \text{start}$

RETURN E, t

A. Results

Figure 11(a) shows that it is on average $1.05\times$ faster to use a C++ uniform random number generator than a C++ lognormal random number generator. Running the program assuming that the lognormal samples are generated by the hardware random number generator in the same amount of time required for a memory access is up to $1.99\times$ faster and always at least $1.26\times$ faster than using the C++ lognormal random number generator. Figure 11(b) shows that the error reduction for the Monte Carlo integration using the $[0, 3]$ C++ uniform random number generator plateaus at around 10^4 samples but for the hardware lognormal the error continues to decrease. The lognormal and $[0, 3]$ C++ uniform lines intersect at between 10^5 and 10^6 samples and the intersection point shifts to the right as we increase the range of the C++ uniform random number generator.

B. Insights from Monte Carlo Integration

Figure 11(b) shows that increasing the range of the C++ uniform random number generator decreases the minimum error that the integration plateaus at. Unfortunately, increasing the range of the C++ uniform random number generator also increases the number of samples required for the estimate of the area to approach the true value. The proportion of the uniform probability density function overlapping the lognormal probability density function increases as the range of the uniform distribution is increased. For example, the overlap of the $[0, 3]$ uniform distribution and $f(x)$ is smaller than that for the $[0, 10]$ uniform distribution and $f(x)$. Therefore, the error can never be zero with any uniform distribution other than $[0, \infty]$ as the source of samples for the numerical integration of $f(x)$. For a given function we cannot know beforehand which

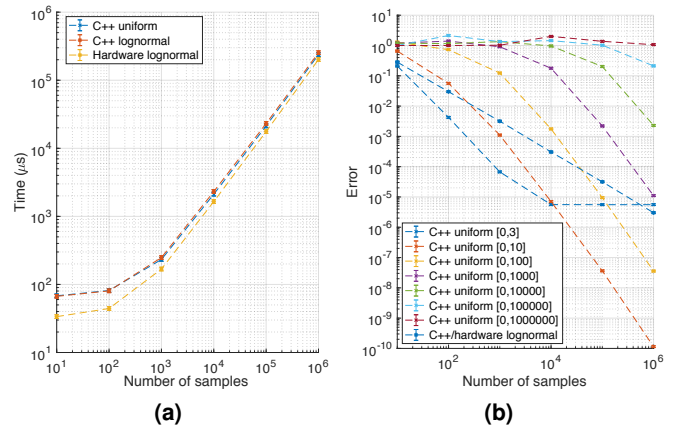


Fig. 11. (a) Time taken to perform a Monte Carlo simulation for N samples using the C++ uniform and lognormal random number generators and the proposed hardware random number generator.; (b) Error in the numerical integration produced by a Monte Carlo simulation for N samples using the C++ uniform and lognormal random number generators. The error bars show a 90 % confidence interval on the mean of 1000 samples for each point.

range of uniform random numbers will produce a sufficiently small bound on the error of integration. The sharp cut-off of the uniform distribution will always cause us to miss some of the area under $f(x)$ that we want to integrate. We can avoid this problem by sampling from the smooth lognormal density that we want to integrate. When performing the Monte Carlo integration of any non-uniform distribution we should sample from the probability density function of that distribution with the same parameters to minimise the error and number of samples required to get a reasonable estimation. This is not possible when sampling from a bounded uniform distribution.

C. The Accept-Reject Method and Computational Cost

The computational complexity of the operations we perform in Algorithm 1 with the exception of the sort have computational cost $\mathcal{O}(N)$ where N is the number of samples. The computational cost of sorting is $\mathcal{O}(N \log(N))$. We expect larger performance gains for integration schemes that do not require a sort operation. Future work will use area-based “dart throwing” integration schemes that avoid sorting.

We have shown that it is better to integrate $f(x)$ with samples from a non-uniform distribution with a similar shape. The accept-reject method is the most flexible software method for generating samples from an arbitrary non-uniform distribution. The method works by transforming samples from a uniform distribution (that the computer can directly generate samples from) to a target non-uniform distribution. We choose to accept or reject samples based on a probabilistic comparison between a uniform random sample and the ratio of the target and uniform probability density functions. As this comparison is probabilistic, it is possible to become stuck rejecting samples forever [6].

VII. RELATED RESEARCH

A hardware random number generator, integrated in a CPU capable of producing samples from arbitrary distributions does not currently exist. Table I shows the state-of-the-art of hardware non-uniform random number generators. The prior

work on non-uniform random number generation in Table I is fundamentally different to prior work on uniform random number generation. The publications in Table I characterise the non-uniform distribution of the physical process used to obtain the random samples. The prior work on uniform random number generators does not produce or refer to a non-uniform distribution of random numbers [19], [31], [34], [40]. The uniform random number generation efforts excluded from Table I produce single-bit samples where the result is either 0 or 1. The non-uniform random number generation efforts included in Table I produce multiple (usually 6 or greater) bit samples with a given non-uniform distribution. There is only one prior work from this decade that is capable of producing samples from arbitrary non-uniform distributions [29]. Their method is not well-suited for integration with current CPU architectures as it requires large optical components. In contrast, Section III describes how the GFET random number generator would interface with an existing CPU.

Beyond its application to Monte Carlo methods, the GFET-based non-uniform random number generator could also see use in other compute-intensive analyses [3], as well as in techniques that trade fidelity of their results for lower power dissipation [35].

Our approach and the approach by Nguyen et al. [29] differ from the state-of-the-art in the following important way: They are programmable to allow an arbitrary distribution to be achieved. In contrast, most of the designs in Table I are not programmable [1], [10], [14], [22], [23], [30], [32], [39], [42]. These are only capable of producing samples from one type of distribution and can only do this for one set of fixed parameters, so would require external modification to make them programmable.

In contrast, Zhang et al. [43] can produce an exponential distribution with any parameters, but would require external modification to produce samples from distributions with different shapes. The work by Hu et al. [12] and Meech et al. [26] can produce samples from a normal distribution with any parameters but would require external modification to allow them to produce samples from distributions with different shapes. The non-programmable random number generators in Table I were designed to suit applications such as cryptography which are drastically different to the applications we propose for our architecture.

Currently no architecture exists with a Gb/s generation rate for arbitrary non-uniform distributions. As the method we present is analog, it should be possible to use existing technology to drive and sample from it. This will allow us to produce samples from arbitrary distributions at Gb/s sample rates. Popular statistical tests such as Dieharder are designed for samples from a [0, 1] uniform distribution and are therefore not compatible with the non-uniformly distributed random numbers produced in this work [2].

A. Alternative Devices

Reconfigurable FETs (RFETs) based on nanowires also possess tunable characteristics: printed multi- and parallel nanowire

TABLE I
STATE-OF-THE-ART IN UNIFORM AND NON-UNIFORM RANDOM NUMBER GENERATION ARCHITECTURES. IN CONTRAST TO THE METHODS BELOW, THE METHOD WE PRESENT IN THIS PAPER GENERATES ARBITRARY DISTRIBUTIONS AND IS ONLY LIMITED BY THE SPEED OF AVAILABLE ANALOG-TO-DIGITAL CONVERTERS (ADCs).

Architecture	Speed	Distribution(s)	Year	Paper
Memristor	6.00 kb/s	Unnamed	2017	[14]
Photon Detection	1.77 Gb/s	Exponential	2017	[23]
FRET	2.89 Gb/s	Exponential	2018	[43]
Photo Diode	17.4 Gb/s	Husumi	2018	[1]
Photon Detection	66.0 Mb/s	Arbitrary	2018	[29]
Photon Detection	200 Mb/s	Normal	2018	[32]
Photon Detection	320 Mb/s	Exponential	2018	[39]
Electronic Noise	6.40 Gb/s	Normal	2019	[12]
Photon Detection	6.80 Mb/s	Exponential	2019	[30]
Photon Detection	63.5 Mb/s	Exponential	2019	[22]
Photon Detection	8.25 Mb/s	Normal	2019	[10]
Photon Detection	1.00 Mb/s	Exponential	2019	[42]
Electronic Noise	13.8 kb/s	Normal	2020	[26]

Schottky barrier devices have similar transfer characteristics to GFETs, where the majority carriers are determined by the gate voltage. FinFETs may also be of interest, as their multi-gate structure allows for tunable characteristics, although not in the same manner as with GFETs or RFETs. FETs based on carbon nanotubes (CNTs) also may have properties of interest, however these also have a number of well-documented issues with scalability and uniformity which limits their prospects of commercialisation.

FinFETs on a 14 nm CMOS process were used by Matthew et al. for a hardware RNG [24], with a throughput on the order of a few hundred Mb/s, however it can only produce samples from a Gaussian distribution, so it is not programmable in the way that ours is. A CNT-based RNG was demonstrated by Rojas et al. in 2017 [7], however no data on the sample rate was produced, and the generated distribution is uniform. A nanowire-based RNG was demonstrated by He et al. [11], however this had a generation rate of less than 10 Mb/s and also involved superconducting properties, requiring operation at temperatures of a few degrees Kelvin and making them impractical for mainstream use.

VIII. SUMMARY AND INSIGHTS

This article demonstrates a novel circuit-level approach to generating samples from non-uniform probability distributions, exploiting the transfer characteristics and ambipolarity of graphene field-effect transistors (GFETs).

We describe the fabrication of arrays of GFETs on a silicon substrate and wire bonding of the fabricated devices to a custom PCB. We experimentally characterise the GFET transfer and output characteristics at a range of GFET V_{DS} bias voltage configurations. Using the obtained characterisation data, we simulate possible circuit designs for PRVAs comprising circuits requiring just two transistors and a resistor (or transimpedance amplifier). The results demonstrate that a circuit comprising a chain of two GFETs transforms a uniformly distributed random input voltage into a non-uniformly distributed output.

We evaluate the end-to-end use of the GFET-circuit-generated distributions in an application performing Monte Carlo integration. The results show that, using the GFET-circuit-generated

non-uniform distributions instead of uniform random samples for sampling locations in the lognormal distribution improves the speed of Monte Carlo integration by a factor of up to $2 \times$. This speedup is based on the assumption that the analog-to-digital converters that will be necessary to read outputs from GFET-based random number generation circuit can produce samples in the same amount of time that it takes to perform memory accesses.

ACKNOWLEDGEMENTS

This research is supported by an Alan Turing Institute award TU/B/000096 under EPSRC grant EP/N510129/1, by EPSRC grant EP/R022534/1, and by EPSRC grant EP/V004654/1. N.J. Tye acknowledges funding from EPSRC grant EP/L016087/1. J.T. Meech acknowledges funding from EPSRC grant EP/L015889/1. We acknowledge contributions from Stephan Hofmann, Jack Alexander-Webber and Ye Fan, as well as funding from Huawei Finland.

REFERENCES

- [1] M. Avesani, D. G. Marangon, G. Vallone, and P. Villoresi. Source-device-independent heterodyne-based quantum random number generator at 17 gbps. *Nature communications*, 9(1):1–7, 2018.
- [2] R. G. Brown. Dieharder. Available at: <http://webhome.phy.duke.edu/~rgb/General/dieharder.php> Accessed 17/04/2020.
- [3] V. Caparrós Cabezas and P. Stanley-Marbell. Parallelism and data movement characterization of contemporary application classes. SPAA '11, page 95–104. ACM, 2011.
- [4] J.-H. Chen, C. Jang, S. Xiao, M. Ishigami, and M. S. Fuhrer. Intrinsic and extrinsic performance limits of graphene devices on sio₂. *Nature Nanotechnology*, 3(4):206–209, 2008.
- [5] I. Daubechies. *Ten Lectures on Wavelets*, pages 53–55. Society for Industrial and Applied Mathematics, Jan. 1992. ISBN: 0898712742.
- [6] L. Devroye. Non-Uniform Random Variate Generation. page 42. Springer-Verlag, McGill University Montreal H3A 2K6 Canada, 1986. ISBN: 1461386454.
- [7] W. A. Gaviria Rojas, J. J. McMorro, M. L. Geier, Q. Tang, C. H. Kim, T. J. Marks, and M. C. Hersam. Solution-processed carbon nanotube true random number generator. *Nano Letters*, 17(8):4976–4981, 2017.
- [8] Graphenea. Graphenea monolayer graphene film on polymer film. https://cdn.shopify.com/s/files/1/0191/2296/files/Graphenea_Monolayer_Graphene_on_Polymer_Film_Datasheet_05-25-2020.pdf?v=1591290809, 2020.
- [9] A. Graps. An introduction to wavelets. *IEEE Computational Science and Engineering*, 2(2):50–61, 1995.
- [10] X. Guo, C. Cheng, M. Wu, Q. Gao, P. Li, and Y. Guo. Parallel real-time quantum random number generator. *Optics letters*, 44(22):5566–5569, 2019.
- [11] Y. He, W. Zhang, H. Zhou, L. You, C. Lv, L. Zhang, X. Liu, J. Wu, S. Chen, M. Ren, Z. Wang, and X. Xie. Bias-free true random number generation using superconducting nanowire single-photon detectors. *Superconductor Science and Technology*, 29(8):085005, jun 2016.
- [12] Y. Hu, Y. Wu, Y. Chen, G. C. Wan, and M. S. Tong. Gaussian random number generator: Implemented in fpga for quantum key distribution. *International Journal of Numerical Modelling: Electronic Networks, Devices and Fields*, 32(3):e2554, 2019.
- [13] Intel. Intel® digital random number generator (drng), 2018. Available at: https://software.intel.com/sites/default/files/managed/98/4a/DRNG_Software_Implementation_Guide_2.1.pdf Accessed 17/04/2020.
- [14] H. Jiang, D. Belkin, S. E. Savel'ev, S. Lin, Z. Wang, Y. Li, S. Joshi, R. Midya, C. Li, M. Rao, et al. A novel true random number generator based on a stochastic diffusive memristor. *Nature communications*, 8(1):1–9, 2017.
- [15] J. Kedzierski, P. Hsu, P. Healey, P. W. Wyatt, C. L. Keast, M. Sprinkle, C. Berger, and W. A. de Heer. Epitaxial graphene transistors on sic substrates. *IEEE Transactions on Electron Devices*, 55(8):2078–2085, Aug 2008.
- [16] R. W. Keyes. What makes a good computer device? *Science*, 230(4722):138–144, 1985.
- [17] S. Kullback and R. A. Leibler. On information and sufficiency. *Ann. Math. Statist.*, 22(1):79–86, 03 1951.
- [18] B. Lambert. *A Student's Guide to Bayesian Statistics*, pages 23–50. SAGE, 2018. ISBN: 1473916364.
- [19] K. Lee and M. Lee. True random number generator (trng) utilizing fm radio signals for mobile and embedded devices in multi-access edge computing. *Sensors*, 19(19):4130, 2019.
- [20] M. Lemme. Current status of graphene transistors. 156:499–509, 1 2010.
- [21] L. Liao, J. Bai, R. Cheng, Y.-C. Lin, S. Jiang, Y. Qu, Y. Huang, and X. Duan. Sub-100 nm channel length graphene transistors. *Nano Letters*, 10(10):3952–3956, 10 2010.
- [22] J. Lin, Y. Wang, Q. Cao, J. Kuang, and L. Wang. True random number generation based on arrival time and position of dark counts in a multichannel silicon photomultiplier. *Review of Scientific Instruments*, 90(11):114704, 2019.
- [23] D. G. Marangon, G. Vallone, and P. Villoresi. Source-device-independent ultrafast quantum random number generation. *Physical review letters*, 118(6):060503, 2017.
- [24] S. K. Mathew, D. Johnston, S. Satpathy, V. Suresh, P. Newman, M. A. Anders, H. Kaul, A. Agarwal, S. K. Hsu, G. Chen, and R. K. Krishnamurthy. μ rng: A 300–950 mv, 323 gbps/w all-digital full-entropy true random number generator in 14 nm finfet cmos. *IEEE Journal of Solid-State Circuits*, 51(7):1695–1704, 2016.
- [25] Maxim Integrated. *PIXI, 20-Port Programmable Mixed-Signal I/O with 12-Bit ADC, 12-Bit DAC, Analog Switches, and GPIO*, 2016. Rev. 3.
- [26] J. T. Meech and P. Stanley-Marbell. Efficient programmable random variate generation accelerator from sensor noise. 2020. arXiv:2001.05400.
- [27] I. Meric, M. Y. Han, A. F. Young, B. Ozyilmaz, P. Kim, and K. L. Shepard. Current saturation in zero-bandgap, top-gated graphene field-effect transistors. *Nature Nanotechnology*, 3(11):654–659, 2008.
- [28] N. Metropolis and S. Ulam. The monte carlo method. *Journal of the American statistical association*, 44(247):335–341, 1949.
- [29] L. Nguyen, P. Rechain, Y. M. Sua, and Y.-P. Huang. Programmable quantum random number generator without postprocessing. *Optics letters*, 43(4):631–634, 2018.
- [30] B. K. Park, H. Park, Y.-S. Kim, J.-S. Kang, Y. Yeom, C. Ye, S. Moon, and S.-W. Han. Practical true random number generator using cmos image sensor dark noise. *IEEE Access*, 7:91407–91413, 2019.
- [31] B. Perach et al. An asynchronous and low-power true random number generator using stt-mtj. *IEEE Transactions on Very Large Scale Integration (VLSI) Systems*, 27(11):2473–2484, 2019.
- [32] F. Raffaelli et al. A homodyne detector integrated onto a photonic chip for measuring quantum states and generating random numbers. *Quantum Science and Technology*, 3(2):025003, 2018.
- [33] F. Schwierz. Graphene transistors. *Nature Nanotechnology*, 5(7):487–496, 2010.
- [34] S. Srinivasan et al. 2.4 ghz 7mw all-digital pvt-variation tolerant true random number generator in 45nm cmos. In *2010 Symposium on VLSI Circuits*, pages 203–204. IEEE, 2010.
- [35] P. Stanley-Marbell, V. Estellers, and M. Rinard. Crayon: Saving power through shape and color approximation on next-generation displays. EuroSys '16, pages 11:1–11:17. ACM, 2016.
- [36] D. B. Thomas. Acceleration of financial monte-carlo simulations using fpgas. In *2010 IEEE Workshop on High Performance Computational Finance*, pages 1–6. IEEE, 2010.
- [37] D. B. Thomas, L. Howes, and W. Luk. A comparison of cpus, gpus, and massively parallel processor arrays for random number generation. In *Proceedings of the ACM/SIGDA international symposium on Field programmable gate arrays*, pages 63–72, 2009.
- [38] S. Thrun. Toward robotic cars. *Comm. ACM*, 53(4):99–106, 2010.
- [39] A. Tomasi et al. Model, validation, and characterization of a robust quantum random number generator based on photon arrival time comparison. *Journal of Lightwave Technology*, 36(18):3843–3854, 2018.
- [40] K. Wallace, K. Moran, E. Novak, G. Zhou, and K. Sun. Toward sensor-based random number generation for mobile and iot devices. *IEEE Internet of Things Journal*, 3(6):1189–1201, 2016.
- [41] H. Wang, Y. Wu, C. Cong, J. Shang, and T. Yu. Hysteresis of electronic transport in graphene transistors. *ACS Nano*, 4(12):7221–7228, 2010.
- [42] H. Xu, N. Massari, L. Gasparini, A. Meneghetti, and A. Tomasi. A spad-based random number generator pixel based on the arrival time of photons. *Integration*, 64:22–28, 2019.

- [43] X. Zhang, R. Bashizade, C. LaBoda, C. Dwyer, and A. R. Lebeck. Architecting a stochastic computing unit with molecular optical devices. In *2018 ACM/IEEE 45th Annual International Symposium on Computer Architecture (ISCA)*, pages 301–314. IEEE, 2018.